Article:
Mills, BJW, Tennenbaum, S and Schwartzman, D (2021) Exploring multiple steady states in Earth's long-term carbon cycle. American Journal of Science, 321 (7). pp. 1033-1044. ISSN: 0002-9599

https://doi.org/10.2475/07.2021.01

Exploring multiple steady states in Earth's long-term carbon cycle

Benjamin J. W. Mills[1*], Stephen Tennenbaum[2] and David Schwartzman[3]

[1]School of Earth and Environment, University of Leeds, Leeds LS2 9JT, UK

[2]Department of Biology, Florida International University, Miami FL, USA

[3] Department of Biology, Howard University, Washington DC, USA

*email b.mills@leeds.ac.uk

Abstract

The long-term carbon cycle regulates Earth's climate and atmospheric CO_2 levels over multimillion-year timescales, but it is not clear that this system has a single steady state for a given input rate of CO_2. In this paper we explore the possibility for multiple steady states in the long-term climate system. Using a simple carbon cycle box model, we show that the location of precipitation bands around the tropics and high mid-latitudes, coupled with the response of the terrestrial biosphere to local surface temperature, can result in system bi-stability. Here, maximum CO_2 drawdown can occur when either the tropics or high mid-latitudes are at the photosynthetic optimum temperature of around 25 ºC, and a period of instability can exist between these states. We suggest that this dynamic has influenced climate variations over Phanerozoic time, and that higher steady state surface temperatures may be easier to reach than is commonly demonstrated in simple 'GEOCARB style' carbon cycle models.

Introduction

It is generally understood that the Earth's surface temperature is buffered against changes over geological timescales, with the result that the planet has never become too hot, or too cold for the maintenance of liquid water in the oceans. A key mechanism controlling this climate stability is the weathering of continental silicate rocks, which transfers atmospheric CO_2 into solution, eventually resulting in the precipitation of carbonate minerals, sequestering carbon over million-year timescales (Walker et al., 1981). Warm conditions increase chemical weathering rates, both through enhanced rainfall and runoff, and faster reaction kinetics (Maher et al., 2014; West, 2012), so warm climate results in a stronger CO_2 sink through silicate weathering, which acts to cool climate. Alternatively, under cool climates, weathering rates are suppressed, and CO_2 levels can increase, and thus silicate weathering acts to stabilize climate.

One key uncertainty in the silicate weathering mechanism, and in the study of long-term climate as a whole, is the strength of the climate regulation under different climate states. For example, as the climate warms over the 21st century, it is feared that various positive feedback processes, such as the loss of reflective ice sheets and CO_2-absorbing rainforests, will act to increase rates of warming (e.g. Lenton et al., 2008). These are relatively short term processes, and the general assumption is that following the cessation of human emissions, CO_2 levels will eventually return to preindustrial levels, which could take timescales of hundreds of thousands of years (Archer et al., 2009). However, this scenario assumes that the long-term carbon cycle provides a net negative feedback on planetary temperature at all temperatures but this is not known with much certainty. If other stable states exist then it is a possibility that the anthropogenic rise of atmospheric carbon dioxide could drive the climate into a higher temperature steady-state. It is also then possible that

47 extreme 'hyperthermals' in Earth's past may have required only a moderate change to carbon
48 inputs and outputs.

49

50 **Feedbacks at different global temperatures**

51 Here we explore a candidate mechanism that seems to be capable of driving an
52 instability in long-term climate to the extent that two simultaneous steady-states can be
53 achieved for the same rate of CO_2 input. The mechanism relies on the ability of terrestrial
54 vegetation to amplify silicate weathering rates. Plants (and their symbiotic fungal partners)
55 have been shown to substantially increase the weathering rates of silicate minerals both in the
56 laboratory (Moulton and Berner, 1998; Lenton et al., 2012; Quirk et al., 2015) and in the field
57 (Bormann et al., 1998; Lenton et al., 2001). They do this in a variety of ways: root structures
58 and fungal hyphae physically break apart soil and regolith; fungi exude organic acids which
59 aid in chemical weathering; soil respiration decreases local pH which also aids in mineral
60 dissolution; plant-enhanced transpiration and water cycling increases local precipitation,
61 runoff and soil moisture. The combined impact of these processes contributes to the biotic
62 enhancement of weathering (e.g. a higher weathering rate for a given temperature;
63 Schwartzman and Volk, 1989; Schwartzman, 1999 2002, 2017).

64 Throughout these alterations, the emergence of plants on to the land surface is thought
65 to have increased global weathering intensities substantially and is linked to CO_2 decline that
66 accompanies early land plant evolution (Berner, 1991; 1997). However, the response of
67 terrestrial vegetation to increasing temperature is not necessarily to increase weathering rates.
68 The optimum temperature for photosynthesis is around 25 C, and at warmer temperatures,
69 efficiency of energy production by plants diminishes. Rising temperatures also increase rates
70 of plant respiration, and increase water stress. Even in the absence of changes to

71 precipitation, present day tropical forests like the Amazon, which are currently at yearly
72 average temperatures of around 25 C, are expected to become less productive under rising
73 temperatures (Malhi et al., 2009). Meanwhile, higher latitude and boreal forests are
74 universally expected to become more productive under increasing temperatures (Malhi et al.,
75 2009) as they are currently limited by cold climate rather than lack of rainfall.

76 Given that plant growth is restricted to distinct tropical and high-latitude bands due to
77 the spacing of Earth's atmospheric cells (e.g. Hadley cells) and distribution of precipitation, it
78 might be expected that global silicate weathering is maximised when each of these
79 precipitation bands is at the optimum temperature for plant growth, a concept summarised in
80 Figure 1. For example, during the warm climate of the Eocene (see Figure 1b), the tropics
81 were some 10 ºC warmer than today, and the photosynthetic optimum temperature of ~25 ºC
82 was shifted to North America and Northern Europe (Tierney et al., 2015), which did see
83 'tropical' rainforest growth, while the African tropics instead hosted savannah and shrubland
84 (Jacobs and Herendeen, 2004). Thus it seems reasonable to expect that a substantially warmer
85 world, as existed for much of the Phanerozoic, would have a very different pattern of plant
86 productivity and silicate weathering.

87 Presently, the vast majority of global silicate weathering occurs in the tropics. In
88 Figure 2 we calculate the global silicate weathering rate at 0.5 degree resolution using the
89 parametric model of West (2012) in conjunction with present day temperature (CRU;
90 Mitchell and Jones, 2005), runoff (Fekete et al., 2002), and topography (NASA SRTM; Farr
91 et al., 2007) fields, following exactly the method defined in Maffre et al. (2018). In this
92 calculation, which is visually similar to previous efforts to constrain global silicate
93 weathering rates (Hilley and Porder, 2008), only 15% of global silicate weathering happens at
94 latitudes more than 40 degrees from the equator, i.e. outside of the tropical precipitation
95 bands. Thus, it is possible that a decline in the efficiency of low-latitude silicate weathering

96 would substantially alter the global long-term carbon sink, potentially leading to instability
97 and positive feedback until the planet warms sufficiently that the high latitude silicate
98 weathering sink becomes more effective.

99

100 **A simple carbon cycle model**

101 To test the possibility for positive feedbacks and multiple steady states in the long-
102 term carbon-climate system we build a simple model based on the canonical GEOCARB
103 framework (Berner, 1991). Despite their age and simplicity, models of this kind are still
104 commonly used to infer Phanerozoic temperature and CO_2 evolution, given that more
105 advanced spatially-explicit modelling cannot be run over the timescales required (Lenton et
106 al., 2018). We solve the following differential equation for the global inorganic carbon
107 balance, where A is total ocean plus atmosphere carbon:

108 $$\frac{dA}{dt} = F_{degass} + F_{carbw} - F_{deposition} \quad (1)$$

109 Here the carbon sources are tectonic CO_2 degassing and carbonate weathering, and the sink is
110 deposition and burial of carbonate minerals. We do not include the organic carbon cycle in
111 this model and assume it is in steady state, as required by the long-term stability of
112 atmospheric oxygen levels. Degassing is represented by a present day rate and a scaling
113 parameter *D*, which we alter between 0.5 and 2 times present day, broadly sampling the
114 expected Phanerozoic range (e.g. Mills et al., 2017):

115 $$F_{degass} = k_{degass} \cdot D \quad (2)$$

116 Carbonate deposition is assumed to equal the rates of silicate plus carbonate weathering to
117 maintain ocean alkalinity balance (e.g. Berner, 1991):

118 $$F_{deposition} = F_{carbw} + F_{silw} \quad (3)$$

119 Thus the carbon balance can be rewritten:

120 $$\frac{dA}{dt} = F_{degass} - F_{silw} \quad (4)$$

121 We depart from the more traditional approach by including a simplified treatment of low and
122 high latitude weathering fluxes, with each responding to the local temperature.

123 $$F_{silw} = F_{sil,low} + F_{sil,high} \quad (5)$$

124 The high and low latitude fluxes are calculated as a product of the overall present day
125 weathering rate (k_{sil}), the fraction of present day weathering that occurs at either high or low
126 latitude (x_j), the relative vegetation mass at that latitude (V_j) and the kinetic effect of local
127 temperature on weathering (f_{T_j}). We split the effects from 'forested' and 'nonvascular'
128 weathering, assuming that nonvascular weathering (e.g. lichens, bryophytes, cyanobacterial
129 mats) would be around 25% as efficient (k_plant = ¼ e.g. Berner and Kothavala, 2001) and
130 that it is the loss of forests that occurs at high temperatures rather than the loss of all biotic
131 weathering. Note that we assume different temperature dependencies for the 'forested' versus
132 'nonvascular' weathering and do not combine these effects.

133 $$F_{sil,j} = k_{sil} \cdot x_j \left(\left(1 - k_{plant}\right)V_j + k_{plant} \cdot f_{T_j} \right) \quad (6)$$

134 Vegetation mass for each latitude band is calculated as a normal distribution ratio dependent
135 on local temperature (T_j), a photosynthetic optimum ($P_{opt} = 25$) and an assumed standard
136 deviation (σ) which controls the function width. This approach follows other carbon cycle
137 modelling (Lenton et al., 2018), but using local instead of global temperature.

138 $$V_j = \frac{norm(T_j, P_{opt}, \sigma)}{norm(T_{j_0}, P_{opt}, \sigma)} \quad (7)$$

For simplicity, we limit the relative biosphere mass in the high latitudes to around 3 times the present day value (k_{biomax} = 3) so that it does not exceed the current tropical biomass, which we assume is close to optimal.

Temperature effects on silicate weathering kinetics follow Berner (1994):

$$f_{T_j} = e^{k_{s1}\left(T_j - T_{j_0}\right)} \cdot \left(1 + k_{s2} \cdot \left(T_j - T_{j_0}\right)\right)^{0.65} \quad (8)$$

Local surface temperature at each latitude band is calculated from the change in global average temperature, ΔT_G as follows:

$$T_{high} = T_{high_0} + \frac{6}{5}\Delta T_G - \frac{1}{5}\frac{\Delta T_G^2}{\Delta T_G + 25} H(\Delta T_G) \quad (9)$$

$$T_{low} = T_{low_0} + \frac{3}{5}\Delta T_G + \frac{2}{5}\frac{\Delta T_G^2}{\Delta T_G + 25} H(\Delta T_G) \quad (10)$$

$$\text{where } H(\Delta T_G) = \begin{cases} 0 \text{ if } \Delta T_G \leq 0 \\ 1 \text{ if } \Delta T_G > 0 \end{cases}$$

This embodies the assumption that tropical temperatures will change by around half as much as polar temperatures due to poleward heat transport (e.g. Cramwinckel et al., 2018). We assume high latitude temperature scales twenty percent faster than the global average and low latitude temperature scales forty percent slower than the average global temperature when it is near or below current values. As the global average increases above current values the high and low latitude changes approach the average rate asymptotically (equations 9 and 10). Global average surface temperature follows a static 'Earth System Sensitivity' ($k_{ESS} = 5\ K$) to CO_2 doubling:

$$\Delta T_G = k_{ESS}\left(\frac{\log RCO_2}{\log 2}\right) \quad (11)$$

Relative atmospheric CO_2 concentration, RCO_2, is calculated from the ocean-atmosphere carbon reservoir assuming that the atmospheric fraction of total carbon increases linearly with

160 total carbon content, thus atmospheric CO_2 concentration is quadratic in A (Kump and
161 Arthur, 1999). Thus:

162 $$RCO_2 = \left(\frac{A}{A_0}\right)^2 \quad (12)$$

163 All constants used in the above follow previous carbon cycle models (Berner, 1994; Lenton
164 et al., 2018) and are shown in table 1. Fractions of 'low' and 'high' latitude weathering are
165 derived here (see Fig. 2) and are taken as 0.85 and 0.15 respectively.

Variable	Description	Value	Units
j	Denotes latitude band	High, low	
A_0	Total ocean & atmosphere carbon	3.2×10^{18}	Mol C
T_j	Local average temperature	$T_{low,0} = 25$; $T_{high,0} = 10$	C
k_{sil}	Global silicate weathering rate	15×10^{12}	Mol C yr^{-1}
k_{degass}	Global tectonic degassing rate	15×10^{12}	Mol C yr^{-1}
k_{s1}	Silicate weathering rate parameter 1	0.0724	
k_{s2}	Silicate weathering rate parameter 2	0.038	
k_{ESS}	Earth system sensitivity to doubling CO_2	5	C
P_{opt}	Plant growth optimal temperature	25	C
σ	Width of plant temperature response	5	C
x_j	Local fraction of global weathering	$x_{low} = 0.85$, $x_{high} = 0.15$	

166

167 ***Table 1.*** *Model parameters.*

168

169 **Model results**

170 Model steady states are shown in Figure 3 and Figure 4, where dotted lines show
171 unstable steady states and solid lines show stable steady states. In the plots shown, the
172 temperature response of the terrestrial biosphere is assumed to be relatively sharp, and
173 follows a normal distribution with a standard deviation of 5 – corresponding to a maximum
174 temperature tolerance of around 40 ºC. In Figure 3 the different line colours show the effect
175 of changing the assumed maximum mass of the high-latitude plant biosphere. Here, a larger

number results in more negative feedback in the system, and delays the collapse of the low latitude biosphere. As the degassing rate increases, a transition occurs at around D = 1.1-1.4 where the low latitude terrestrial biosphere collapses and regulation shifts to the higher latitudes. When initiated at high CO_2 levels, the high latitude biosphere is able to maintain stability as CO_2 input decreases beyond the initial transition point. This demonstrates hysteresis and both a lower temperature steady state and an upper temperature steady state are viable for some values of D. Widening the biosphere temperature response by increasing the standard deviation for the temperature function dampens this dynamic and eventually eliminates hysteresis, although the feedback strength remains variable. Note that a further transition occurs at temperatures above 40 ºC where the high-latitude vegetation collapses. Figure 4 demonstrates that when the assumed contribution of the plant biosphere to weathering is larger, the degree of hysteresis which can be generated is also larger.

Discussion

This is a simplistic analysis that shows how positive feedbacks in the long-term carbon cycle can lead to nonlinear responses of global silicate weathering to temperature change, and to the possibility of upper temperature steady states. Although the use of the normal function to represent vegetation-temperature response masks a great deal of complexity, the qualitative dynamics are hard to avoid: At some global temperature Earth's tropical vegetation will start to decline, and this will shift the burden of biologically-assisted weathering (as well as direct CO_2 drawdown) to the higher latitudes, changing the silicate weathering feedback. Established models of the long-term carbon cycle (Berner, 2006; Lenton et al., 2018) tend to assume that global vegetation will provide a negative feedback on CO_2 increases as average surface temperature rises (at least up to ~25 ºC). However, this is

200 likely not the case, and a weakening of this negative feedback should make higher surface
201 temperatures easier to achieve.

202 A great many technical challenges remain in testing the existence of multiple steady
203 states in Earth's long-term carbon cycle: such a test requires a spatially-resolved model that
204 can incorporate changing climate and vegetation dynamics, and can infer their effects on
205 weathering and carbon burial over multi-million year timescales. The GEOCLIM model
206 (Godderis et al., 2014) includes a representation of climate and terrestrial vegetation, but not
207 the biotic effect on weathering. The linked SDGVM-HadCM3L approach used by Taylor et
208 al. (2012) does link climate, vegetation and weathering, but would need to be expanded to
209 include a range of different CO_2 levels in the GCM to test this idea. Part of the motivation for
210 developing the SCION continuous climate-biogeochemical model (Mills et al., 2021) is to aid
211 in testing hypotheses like this, but that model does not yet include dynamic vegetation. It is
212 hoped that a 3D approach will be able to explore this idea in the near future.

213 The simple approach here ignores several negative feedbacks which may help buffer
214 against runaway climate change (such as nutrient cycling and changes to the global oxygen
215 reservoir), but it also does not incorporate other positive feedbacks which might exacerbate
216 the situation, such as a runoff or temperature controls on organic carbon oxidation, which
217 should amplify long-term warming. Overall, it seems very unlikely that the Earth responds to
218 warming in the same way across all global temperatures and background states, and the
219 existence of various 'temperature-attractors' should be considered when reconstructing the
220 long-term system. The attractors may also depend on the distribution of the continents and
221 the availability of 'weatherable' land (e.g. Godderis et al., 2014) and sufficient precipitation
222 (e.g. Hasegawa et al., 2012) at different latitudes, as well as the degree of biological
223 enhancement of weathering. Overall, this work should be seen as an initial exploration of the

qualitative dynamics, and the thresholds for an upper temperature steady state on Earth may be very different to those in our simple model.

Looking to the geological record, the Early Triassic may be the best possible example of an upper temperature steady state. Here, low latitude surface ocean temperatures are estimated to have been around 36-40 ºC (Sun et al., 2012), following the emplacement of the Siberian Traps around the P-T boundary. Interestingly, the warm period persists for at least 5 million years, far longer than the expected time for the system to restore equilibrium following a CO_2 input event (estimated to be around 50 kyrs by Clarkson et al., 2015). It has been suggested that the early Triassic may have seen a failure of climate regulation (Kump, 2018) where CO_2 input overwhelmed the global availability of silicate rocks, although the carbonate $\delta^{13}C$ record does not show the persistent positive excursion that other models for 'maxed out' weathering rates have predicted (Mills et al., 2011). It may be possible that a steady state was reached in several 10s or 100s of kyrs, only this was an Upper Temperature Steady State under a different silicate weathering regime, something seemingly consistent with the loss of tropical forests at this time and the shift of these species to higher latitudes (Sun et al., 2012). Furthermore, the mid-Cretaceous climate reached temperatures of roughly 35 °C at the equator and 25 °C at latitude 60 N (Hu et al., 2012). Evidence of temperate rainforests near the South Pole at this time (Klages et al., 2020) points to the possibility that the mid-Cretaceous climate is also an example of an Upper Temperature Steady State. A reversion to a lower temperature steady state following these events could be achieved by a relatively small downward adjustment in degassing rates, as shown in our model.

Acknowledgements

We thank the editors and reviewers for their constructive remarks. BJWM is funded by the UK Natural Environment Research Council (NE/S009663/1).

Author Contributions

All authors contributed to the design of the study, the model, and the writing of the paper.

Appendix – model code transcription

The code for this model is very simple. The part of the MATLAB script containing the main equations is included below for reference. Full code can be downloaded at https://github.com/bjwmills

```
%%%% CO2 and global avg. surface temp
RCO2 = (A/pars.A0)^2;
climsens = 5 ;
GAST_0 = 15 ;
GAST = GAST_0 + climsens*(log(RCO2)/log(2)) ;

%%%% high lat and low lat T
DGT = GAST-GAST_0;
HGT = heaviside(DGT);
T_hilat_0 = 10 ;
T_hilat = T_hilat_0 + 1.2*DGT - 0.2*HGT.*(DGT.^2)./(DGT+25);
T_lowlat_0 = 25 ;
T_lowlat = T_lowlat_0 + 0.6*DGT + 0.4*HGT.*(DGT.^2)./(DGT+25);

%%%% biota effects
Gmean = 25 ;
Gsd = 5 ;
f_biota_hilat = min( normpdf(T_hilat,Gmean,Gsd)./normpdf(T_hilat_0,Gmean,Gsd) ,2.5 ) ;
f_biota_lowlat = min( normpdf(T_lowlat,Gmean,Gsd)./normpdf(T_lowlat_0,Gmean,Gsd) ,
2.5 ) ;

%%%% weathering T effects
f_T_hilat =  exp(0.0724*(T_hilat - T_hilat_0)) * ( (1 + 0.038*(T_hilat - T_hilat_0))^0.65 ) ;
if isreal(f_T_hilat) == 0
    f_T_hilat = 0 ;
end
g_T_hilat = 1 + 0.087*(T_hilat - T_hilat_0) ;
f_T_lowlat =  exp(0.0724*(T_lowlat - T_lowlat_0)) * ( (1 + 0.038*(T_lowlat -
T_lowlat_0))^0.65 ) ;
```

```
if isreal(f_T_lowlat) == 0
   f_T_lowlat = 0 ;
end
g_T_lowlat = 1 + 0.087*(T_lowlat - T_lowlat_0) ;

%%%% weathering fluxes
lowlatfrac = 0.85 ;
hilatfrac = 1 - lowlatfrac ;
silw_hilat = hilatfrac * pars.k_silw * ( 0.75*f_biota_hilat + 0.25*f_T_hilat );
carbw_hilat = hilatfrac * pars.k_carbw * ( 0.75*f_biota_hilat + 0.25*g_T_hilat ) ;
silw_lowlat = lowlatfrac * pars.k_silw * ( 0.75*f_biota_lowlat + 0.25*f_T_lowlat ) ;
carbw_lowlat = lowlatfrac * pars.k_carbw * ( 0.75*f_biota_lowlat + 0.25*g_T_lowlat ) ;

silw = silw_lowlat + silw_hilat ;
carbw = carbw_lowlat + carbw_hilat ;

%%%% degassing
ccdeg = pars.k_ccdeg * D_input ;
%%%% deposition
mccb = silw + carbw ;

%%%%   Reservoir calculations   %%%%%%

%%%% Ocean-atmosphere carbon (A)
dy(1) = ccdeg + carbw - mccb ;
```

References

Archer, D., Eby, M., Brovkin, V., Ridgwell, A., Cao, L., Mikolajewicz, U., Caldeira, K., Matsumoto, K., Munhoven, G., Montenegro, A., Tokos, K., 2009. Atmospheric Lifetime of Fossil Fuel Carbon Dioxide. Annual review of Earth and planetary sciences 37, 117-134.

Berner R.A. (1991) A model for atmospheric CO2 over Phanerozoic time. Amer. J. Sci. 291, 339-376.

Berner, R.A., 1994. Geocarb II: A revised model of atmospheric CO2 over Phanerozoic time. American Journal of Science 294, 56-91.

Berner, R.A., 1997. The Rise of Plants and Their Effect on Weathering and Atmospheric CO2. Science 276, 544-546.

323 Berner, R.A., 2006. GEOCARBSULF: A combined model for Phanerozoic atmospheric O2
324 and CO2. Geochimica et Cosmochimica Acta 70, 5653-5664.

325 Berner, R.A., Kothavala, Z., 2001. Geocarb III: {A} revised model of atmospheric CO2 over
326 Phanerozoic time. American Journal of Science 301, 182-204.

327 Bormann, B.T., Wang, D., Bormann, F.H., Benoit, G., April, R., Snyder, M.C., 1998. Rapid,
328 plant-induced weathering in an aggrading experimental ecosystem. Biogeochemistry 43,
329 129-155.

330 Clarkson, M.O., Kasemann, S.A., Wood, R.A., Lenton, T.M., Daines, S.J., Richoz, S.,
331 Ohnemueller, F., Meixner, A., Poulton, S.W., Tipper, E.T., 2015. Ocean acidification and
332 the Permo-Triassic mass extinction. Science 348, 229-232.

333 Cramwinckel, M.J., Huber, M., Kocken, I.J., Agnini, C., Bijl, P.K., Bohaty, S.M., Frieling, J.,
334 Goldner, A., Hilgen, F.J., Kip, E.L., Peterse, F., van der Ploeg, R., Rohl, U., Schouten, S.,
335 Sluijs, A., 2018. Synchronous tropical and polar temperature evolution in the Eocene.
336 Nature 559, 382-386.

337 Farr, T. G., et al. (2007), The Shuttle Radar Topography Mission, Rev. Geophys., 45,
338 RG2004, doi:10.1029/2005RG000183.

339 Fekete, B.M., Vörösmarty, C.J., Grabs, W., 2002. High-resolution fields of global runoff
340 combining observed river discharge and simulated water balances. Global biogeochemical
341 cycles 16, 15-11-15-10.

342 Goddéris, Y., Donnadieu, Y., Le Hir, G., Lefebvre, V., Nardin, E., 2014. The role of
343 palaeogeography in the Phanerozoic history of atmospheric CO2 and climate. Earth-
344 Science Reviews 128, 122-138.

345 Hasegawa, H., Tada, R., Jiang, X., Suganuma, Y., Imsamut, S., Charusiri, P., Ichinnorov, N.,
346 and Khand, Y.: Drastic shrinking of the Hadley circulation during the mid-Cretaceous
347 Supergreenhouse, Clim. Past, 8, 1323–1337, 2012.

348 Hilley, G.E., Porder, S., 2008. A framework for predicting global silicate weathering and
349 CO2 drawdown rates over geologic time-scales. PNAS 105, 16855-16859.

350 Hu, X., Wagreich, M. & Yilmaz, I.O. (2012) Marine rapid environmental/climatic change in
351 the Cretaceous greenhouse world. Cretaceous Res. 38, 1-6.

352 Klages, J.P., Salzmann, U., Bickert, T. et al. (2020) Temperate rainforests near the South Pole
353 during peak Cretaceous warmth. Nature 580, 81- 92.

354 Jacobs, B.F., Herendeen, P.S., 2004. Eocene dry climate and woodland vegetation in tropical
355 Africa reconstructed from fossil leaves from northern Tanzania. Palaeogeography,
356 Palaeoclimatology, Palaeoecology 213, 115-123.

357 Kump, L.R., Arthur, M.A., 1999. Interpreting carbon-isotope excursions: carbonates and
358 organic matter. Chemical Geology 161, 181-198.

359 Kump, L.R., 2018. Prolonged Late Permian-Early Triassic hyperthermal: failure of climate
360 regulation? Philos Trans A Math Phys Eng Sci 376.

361 Lenton, T.M., 2001. The role of land plants, phosphorus weathering and fire in the rise and
362 regulation of atmospheric oxygen. Global Change Biology 7, 613-629.

363 Lenton, T. M., et al., 2008. Tipping elements in the Earth's climate system. PNAS 105, 1786-
364 1793.

365 Lenton, T.M., Crouch, M., Johnson, M., Pires, N., Dolan, L., 2012. First plants cooled the
366 Ordovician. Nature Geoscience 5, 86-89.

367 Lenton, T.M., Daines, S.J., Mills, B.J.W., 2018. COPSE reloaded: An improved model of
368 biogeochemical cycling over Phanerozoic time. Earth-Science Reviews 178, 1-28.

369 Maffre, P., Ladant, J.-B., Moquet, J.-S., Carretier, S., Labat, D., Goddéris, Y., 2018.
370 Mountain ranges, climate and weathering. Do orogens strengthen or weaken the silicate
371 weathering carbon sink? Earth and planetary science letters 493, 174-185.

372 Maher, K., Chamberlain, C.P., 2014. Hydrologic regulation of chemical weathering and the
373 geologic carbon cycle. Science 343, 1502-1504.

374 Malhi, Y., Aragao, L. E. O. C., Galbraith, D., Huntingford, C., Fisher, R., Zelazowski, P.,
375 Sitch, S., McSweeney, C., Meir, P. Exploring the likelihood and mechanism of a climate-
376 change-induced dieback of the Amazon rainforest. PNAS 106, 20610-20615.

377 Mills, B., Watson, A.J., Goldblatt, C., Boyle, R., Lenton, T.M., 2011. Timing of
378 Neoproterozoic glaciations linked to transport-limited global weathering. Nature
379 Geoscience 4, 861-864.

Mills, B.J.W., Scotese, C.R., Walding, N.G., Shields, G.A., Lenton, T.M., 2017. Elevated CO2 degassing rates prevented the return of Snowball Earth during the Phanerozoic. Nat Commun 8, 1110.

Mitchell, T.D., Jones, P.D., 2005. An improved method of constructing a database of monthly climate observations and associated high-resolution grids. International Journal of Climatology 25, 693-712.

Moulton, K. L. & Berner, R. A. Quantification of the effect of plants on weathering: Studies in Iceland. Geology 26, 895 (1998).

Quirk, J., Leake, J.R., Johnson, D.A., Taylor, L.L., Saccone, L., Beerling, D.J., 2015. Constraining the role of early land plants in Palaeozoic weathering and global cooling. Proc Biol Sci 282, 20151115.

Schwartzman D.W., Volk T (1989) Biotic enhancement of weathering and the habitability of Earth. Nature 340: 457-460.

Schwartzman, D. (1999 2002) Life, Temperature, and the Earth: The Self-Organizing Biosphere. Columbia University Press, New York.

Schwartzman, D. (2017) Life's Critical Role in the Long-term Carbon Cycle: the Biotic Enhancement of Weathering, AIMS Geosciences 3(2): 216 -238.

Sun, Y., Joachimski, M.M., Wignall, P.B., Yan, C., Chen, Y., Jiang, H., Wang, L., Lai, X., 2012. Lethally hot temperatures during the Early Triassic greenhouse. Science 338, 366-370.

Taylor, L. L., Banwart, S. A., Valdes, P. J., Leake, J. R. & Beerling, D. J. Evaluating the effects of terrestrial ecosystems, climate and carbon dioxide on weathering over geological time: a global-scale process-based approach. Philos Trans R Soc Lond B Biol Sci 367, 565-582 (2012).

Tierney, J. E., Sinninghe Damste, J. S., Pancost, R. D., Sluijs, A., Zachos, J. C. Eocene temperature gradients. Nature Geoscience 10, 538-539.

Walker, J.C.G., Hays, P.B., Kasting, J.F., 1981. A negative feedback mechanism for the long-term stabilization of Earth's surface temperature. Journal of Geophysical Research 86, 9776-9782.

409 West, A.J., 2012. Thickness of the chemical weathering zone and implications for erosional
410 and climatic drivers of weathering and for carbon-cycle feedbacks. Geology 40, 811-814.

411

412

413 **Figures and captions**

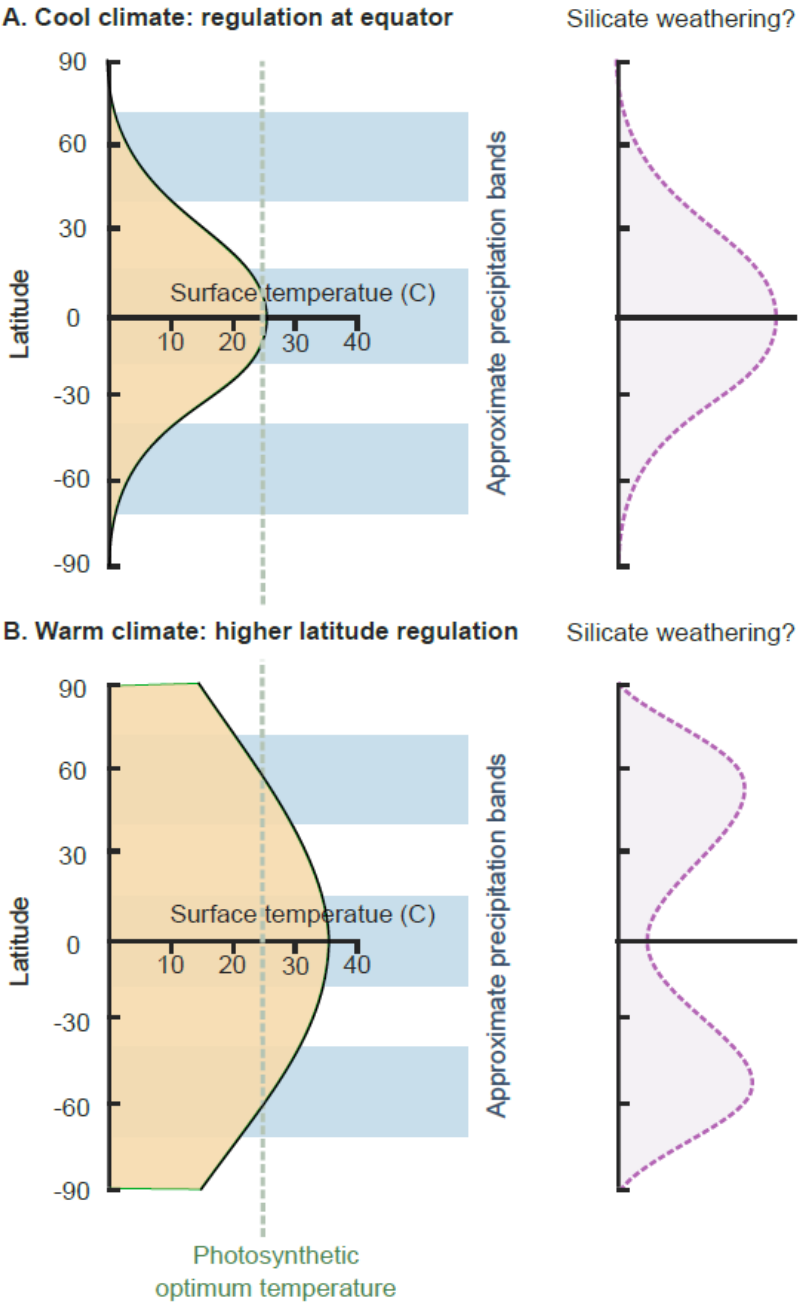

414

415 **Figure 1. Mechanism for climate stabilization at different surface air temperatures.** A.
416 Under cool climate (~15 C shown), photosynthetic optimum temperature coincides with the
417 equatorial precipitation band, and silicate weathering is likely to be enhanced in low latitudes.
418 B. Under warmer climate (~25 C shown) photosynthetic optimum temperature coincides with
419 the other major precipitation bands in the high mid-latitudes, thus silicate weathering could
420 be more prevalent at high latitudes.

421

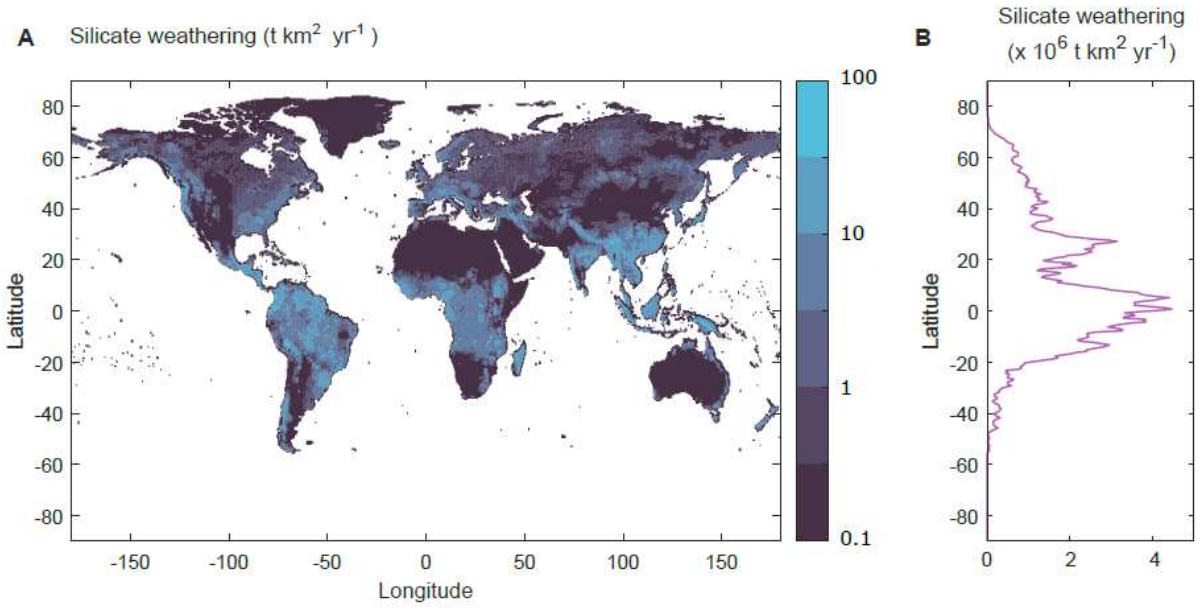

422

423 **Figure 2. Present day chemical silicate weathering distribution showing extent of**
424 **tropical regulation.** A. Estimated silicate weathering rates for the preindustrial Earth. B.
425 Latitudinal plot showing that almost all silicate weathering (~85%) occurs at latitudes less
426 than 40 degrees.

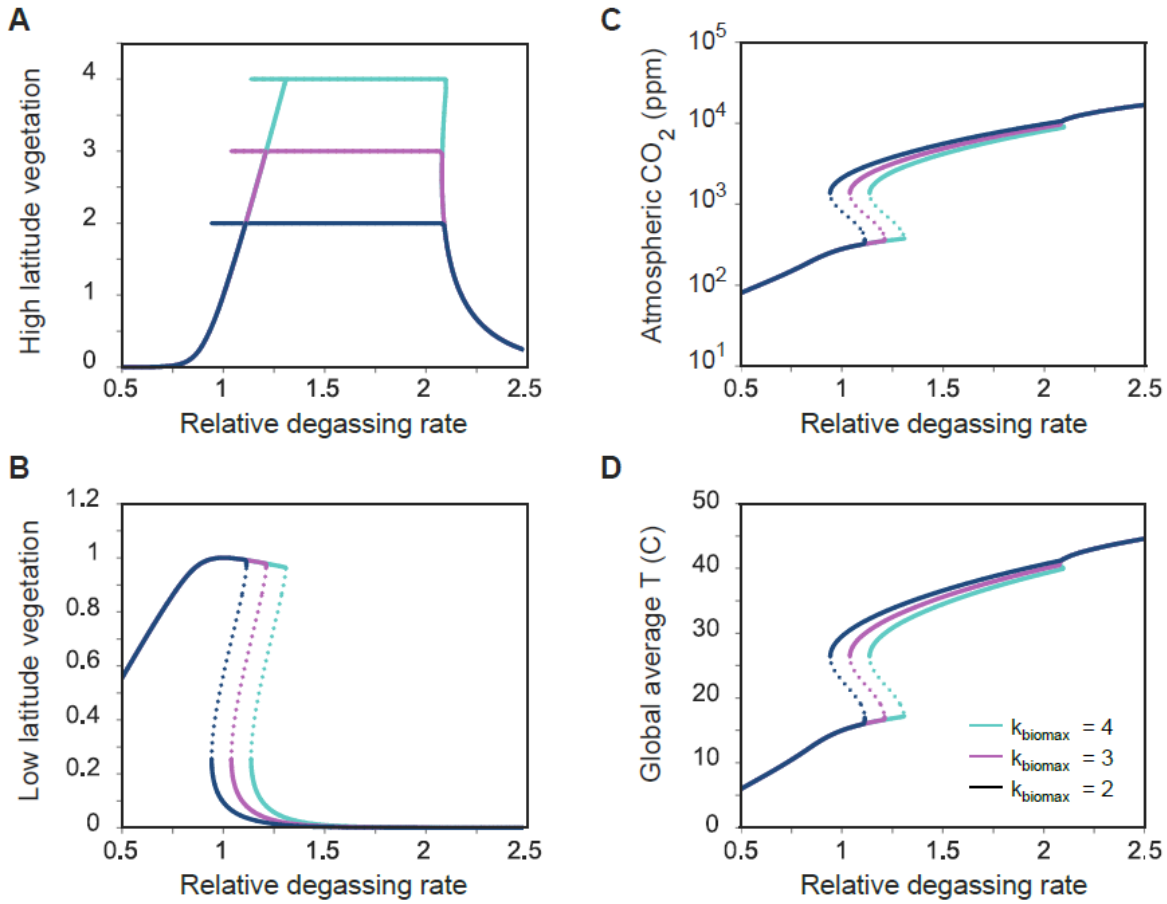

Figure 3. Carbon cycle model steady states under different carbon degassing rates. Solid lines show stable solutions, dotted lines show unstable solutions. A. Relative mass of the high-latitude vegetation (stable and unstable steady-states overlap in the area of constant productivity). B. Relative mass of the low-latitude vegetation. C. Atmospheric CO_2 concentration. D. Global average surface temperature. Line colours show the effect of varying the maximum permitted mass of the high-latitude vegetation, k_{biomax}.

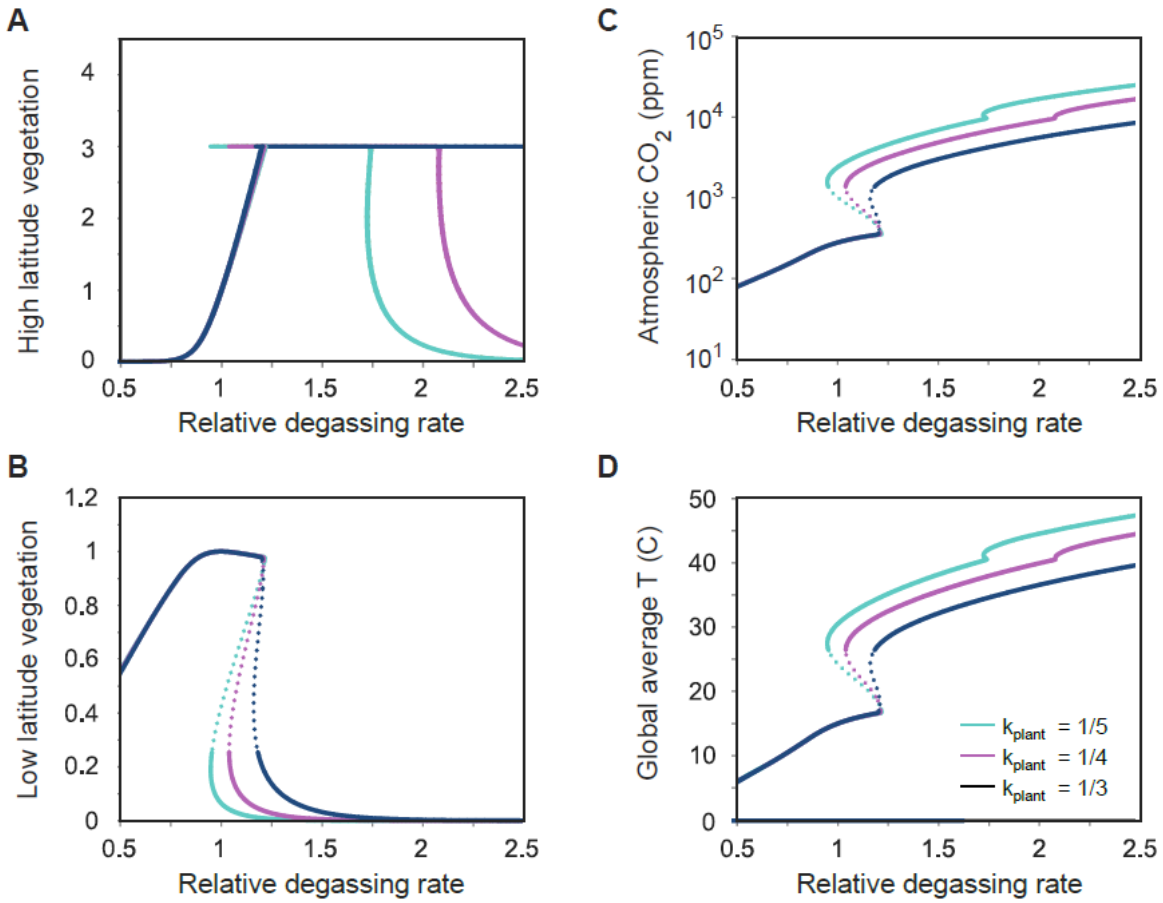

Figure 4. Further carbon cycle model steady states under different carbon degassing rates. Solid lines show stable solutions, dotted lines show unstable solutions. A. Relative mass of the high-latitude vegetation (stable and unstable steady-states overlap in the area of constant productivity). B. Relative mass of the low-latitude vegetation. C. Atmospheric CO_2 concentration. D. Global average surface temperature. Line colours show the effect of varying the plant weathering enhancement factor, k_{plant}.